JCI insight

Allograft inflammatory factor-1 in myeloid cells drives autoimmunity in type 1 diabetes

Diana M. Elizondo,[1,2] Nailah Z.D. Brandy,[1] Ricardo L. da Silva,[1,3] Tatiana R. de Moura,[4] and Michael W. Lipscomb[1]

[1]Department of Biology, Howard University, Washington, DC, USA. [2]Department of Pediatrics, University of Michigan, Ann Arbor, Michigan, USA. [3]Laboratório de Imunologia e Biologia Molecular, Universidade Federal de Sergipe, Aracaju, Brazil. [4]Department of Morphology, Universidade Federal de Sergipe, São Cristovão, Brazil.

Allograft inflammatory factor-1 (AIF1) is a calcium-responsive cytoplasmic scaffold protein that directs hematopoiesis and immune responses within dendritic cells (DC) and macrophages. Although the role of AIF1 in transplant rejection and rheumatoid arthritis has been explored, little is known about its role in type 1 diabetes. Here, we show that in vivo silencing of AIF1 in NOD mice restrained infiltration of immune cells into the pancreas and inhibited diabetes incidence. Analyses of FACS-sorted CD45^{neg} nonleukocyte populations from resected pancreatic islets showed markedly higher expression of insulin in the AIF1-silenced groups. Evaluation of CD45^{+} leukocytes revealed diminished infiltration of effector T cells and DC in the absence of AIF1. Transcriptional profiling further revealed a marked decrease in cDC1 DC-associated genes CD103, BATF3, and IRF8, which are required for orchestrating polarized type 1 immunity. Reduced T cell numbers within the islets were observed, with concomitant lower levels of IFN-γ and T-bet in AIF1-silenced cohorts. In turn, there was a reciprocal increase in functionally suppressive pancreas-resident CD25^{+}Foxp3^{+}CD4^{+} Tregs. Taken together, results show that AIF1 expression in myeloid cells plays a pivotal role in promoting type 1 diabetes and that its suppression restrains insulitis by shifting the immune microenvironment toward tolerance.

Introduction

Type 1 diabetes (T1D) is marked by chronic autoimmune destruction of β cells within pancreatic islets. The pathology is driven by infiltrating antigen-specific autoreactive CD4^{+} helper and CD8^{+} cytotoxic T cells (1). Importantly, antigen-presenting myeloid cells, particularly macrophages and dendritic cells (DC), are responsible for driving the insulitis (2–4).

Resident macrophages within the pancreatic islets are instrumental in directing immune pathology in T1D. Ablation of macrophages using mAb targeting the CSF-1 receptor significantly delayed autoimmune diabetes by reducing presence of insulin epitopes for autoantigen presentation, thereby leading to reduced T cell infiltration (5). A pivotal role of the Batf3-dependent CD103^{+} conventional DC type 1 (cDC1) subpopulation was recently determined to be a principal director of insulitis (2). Additional studies have shown that CD11c^{+}CD11b^{+} DC (or cDC2) subsets also play pivotal roles in directing insulitis (6, 7). Finally, other important work has shown that the majority of infiltrated DC into the islets are not of the Zbtb46 cDC lineage (8) but are monocyte-derived DC (MoDC) in origin (4). Thus, the chronic state of T1D is perpetuated by the feed-forward chronic proinflammatory responses of resident macrophages and the various DC subsets. These antigen-presenting myeloid cell subsets are responsible for driving autoreactive T cells, whereby the imbalance between effector type 1 polarized CD4^{+} T cells versus CD4^{+}CD25^{+}Foxp3^{+} Tregs leads to establishment of T1D (9, 10).

Allograft inflammatory factor-1 (AIF1) is a calcium-responsive scaffold adaptor protein with an EF-hand region that interacts with the actin cytoskeleton and PKC (11, 12). The gene is restricted to antigen-presenting myeloid cells, with expression in cDC1 DC, a minor subset of cDC2, MoDC, and macrophages (12–14). Expression in these subsets is important for directing innate and adaptive immune responses (12, 13, 15–17). Silencing of the gene in DC directly restrains polarized type 1 immune responses (13, 15). Additionally, the protein plays prominent roles in microglial functioning (18) and has been linked to brain inflammation (19).

Reports have shown that AIF1 is involved in several autoimmune disorders, including diabetes, systemic sclerosis (20, 21), rheumatoid arthritis (22, 23), and an experimental autoimmune encephalomyelitis model (24). GWAS showed that polymorphisms within the gene correlated with a higher predisposition rate for diabetes (25, 26). Other reports have shown a correlation between high levels of AIF1 and insulitis in NOD mice (27, 28). However, no study has clearly addressed the causative role of AIF1 in directing insulitis and T1D. In this study, AIF1 was silenced during the early phases of insulitis in NOD mice using in vivo siRNA nonviral delivery approaches to evaluate the contributing role of the protein to autoimmunity and T1D onset. Inhibition of AIF1 restrained insulitis events, promoted long-term survival, and prevented diabetes onset by reducing proinflammatory responses and inhibiting autoreactive T cell infiltration into the pancreas. This was further marked by expansion of pancreas-resident antigen-specific Tregs that assisted in shifting the microenvironment toward that of tolerance.

Results

AIF1 is expressed in myeloid cells within the pancreata of NOD mice. AIF1 expression in CD45+ leukocytes within the pancreata of NOD mice was monitored during insulitis by flow cytometric analysis and real-time PCR. Pancreata from 6-, 9-, 12-, 15-, and 18-week-old NOD mice were harvested before flow cytometric evaluation of AIF1 expression (Figure 1A). Expression of AIF1 was detected in the CD11b+, F4/80+, and CD11c+ subsets pregated on CD45+, which largely comprise the varying macrophages and DC subsets. As anticipated, frequency of these myeloid subsets were reduced as T cell infiltration occurred over successive weeks. As a corroborative approach, transcription levels of AIF1 were assessed by quantitative PCR (qPCR) on sorted populations of CD11c+, F4/80+, CD11c+, or TCR+ subsets derived from the pancreatic islets (Figure 1B). As previously shown by flow cytometric analyses, AIF1 expression was restricted to myeloid cells because no AIF1 was detected in TCR+ T lymphocytes (12). Histological examinations of 12-week-old NOD mice pancreas confirmed colocalization of AIF1 within CD11b and F4/80 subsets (Supplemental Figure 1; supplemental material available online with this article; https://doi.org/10.1172/jci.insight.136092DS1), corroborating published reports of AIF1 coexpression in tissue myeloid populations (12, 29, 30).

In vivo silencing of AIF1 restrains diabetes incidence and reduces immune cell infiltration. After identifying expression of AIF1 in DC and macrophages within the pancreata of NOD mice, we next aimed to suppress expression of the protein in vivo. NOD mice at 6 weeks of age were injected i.p. with siRNA targeting AIF1 (siAIF1) weekly for a total of 3 weeks. Using two different siRNA targeting AIF1, a single i.p. injection was able to suppress AIF1 in CD45+TCRβ− subsets maximally for up to 7 days, relative to injection with scrambled siRNA (siScramble) oligonucleotides as controls (Supplemental Figure 2A). Notably, most AIF1 expression levels were recovered by day 14. after the initial i.p. injection, with no significant reduction in expression within the splenic compartment (Supplemental Figure 2B).

Evaluation of AIF1 protein expression showed that i.p. injection of siAIF1 restrained levels in pancreas myeloid CD11b−CD11c+F4/80− DC and CD11b+F480+ macrophages for 7 days (Supplemental Figure 2C). Both siScramble oligonucleotides and congenic immunodeficient mice on the NOD background (NOD/SCID) served as internal controls. In vivo silencing of AIF1 resulted in approximately 80% of treated NOD mice diabetes free through 60 weeks of age (Figure 2A). Approximately 20% of treated NOD mice that did develop diabetes had delayed onsets 9 ± 2.4 weeks after control groups. Blood glucose monitoring revealed markedly lower levels in siAIF1-silenced groups compared with siScramble controls (Figure 2B). Glucose levels paralleled those of the NOD/SCID group for up to 24 weeks of age (or 18 weeks after treatment by silencing AIF1). Serum measurement of treated mice revealed higher levels of insulin (Figure 2C) along with reduced IFN-γ levels (Figure 2D); data are presented as an aggregate of collected sera from treated versus control mice over 6 to 30 weeks of age.

To assess immune cell infiltration, NOD mice silenced for AIF1 at 15 weeks of age were sacrificed and the pancreata were excised to isolate and interrogate leukocytes. Flow cytometric analyses revealed a 3-fold reduction in percentage of CD45+ immune cells within the pancreas of siAIF1-treated NOD mice (Figure 2E). Further gating on the CD45+ subsets revealed a markedly lower proportion of TCRβ+ T cells, with less frequency of the CD4+TCRβ+ T cells. Interestingly, no significant change in the ratio of CD8+ T cells was reproducibly observed. Next, using flow cytometric sorting, CD45neg and CD45+ cells were isolated from the pancreas of treated versus control groups before measuring gene expression by qPCR (Figure 2, F and G). For the nonimmune CD45neg pancreatic islet cell subsets, gene expression studies revealed significantly
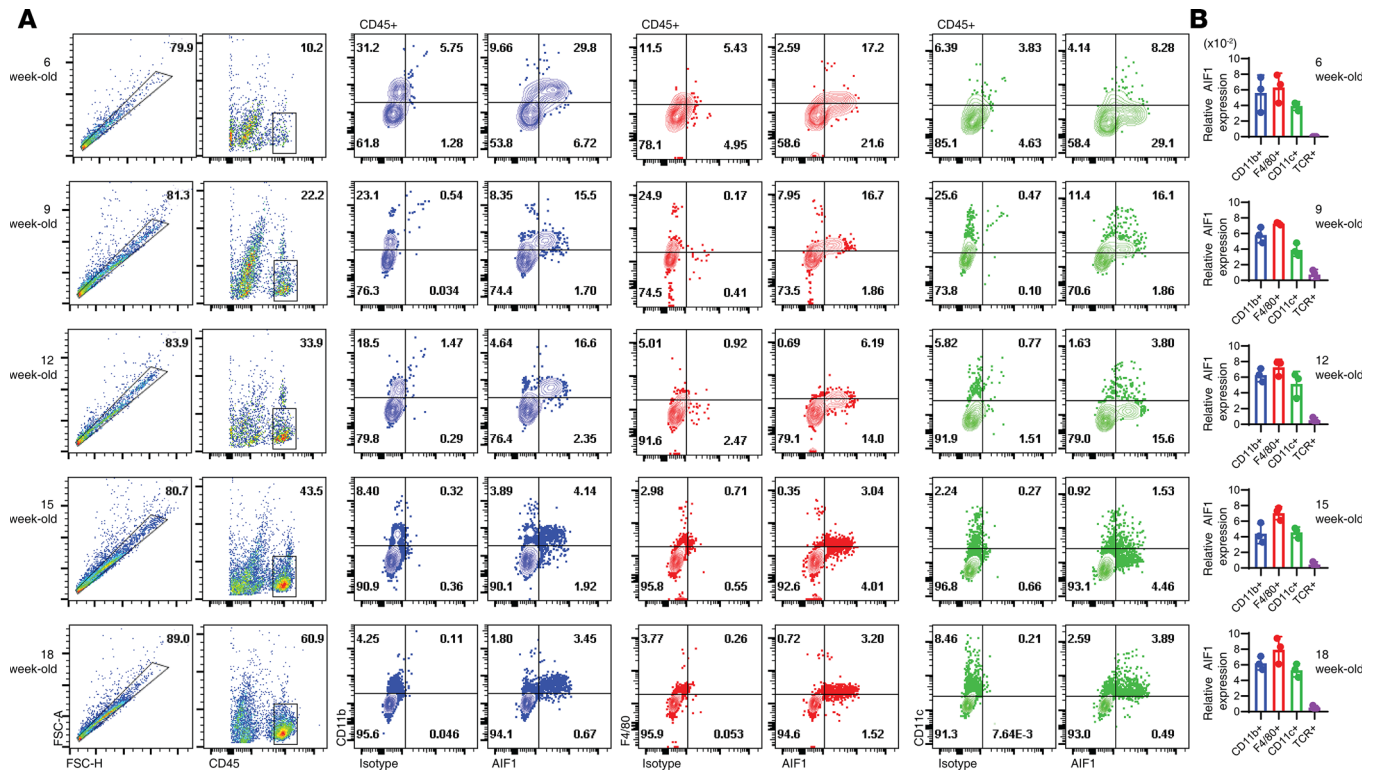
Figure 1. Insulitis progression is marked by expression of AIF1 in DC and macrophages. Pancreas from NOD mice at 6, 9, 12, 15, and 18 weeks were isolated and stained to evaluate AIF1 expression in CD45$^+$ cell subsets. (**A**) FSC-A vs. FSC-H was used to isolate singlets. The CD45$^+$ singlet subsets were then analyzed for coexpression of AIF1 with either CD11b, F4/80, or CD11c. Flow cytometric dot plot data sets are representative of three mice per age group in three independent experiments. (**B**) AIF1 gene expression was analyzed by real-time PCR in NOD pancreatic CD45$^+$ cells flow cytometric sorted for either CD11b$^+$, F4/80$^+$, CD11c$^+$, or TCR$^+$ (TCR) populations. Data represent the mean ± SEM of three mice per age group in three independent experiments normalized for respective internal loading controls. AIF1, allograft inflammatory factor-1.

higher levels of insulin and reduced expression of IL-6 in the siAIF1-treated groups compared with controls. No significant differences in glucagon expression was detected. For the CD45$^+$ sorted population, lower levels of AIF1, CD3, CD11c, and CD11b were detected, along with lower transcripts of cytokines for IFN-γ and IL-21. Finally, histological examination for insulitis corroborated reduced leukocyte infiltration within the islets of the AIF1-silenced cohort relative to siScramble-treated NOD controls (Figure 2H). Taken together, in vivo silencing of AIF1 suppresses insulitis, as shown by reduced infiltration of leukocytes into the pancreas and lower proinflammatory cytokine profiles.

Alterations of the myeloid compartment within the pancreas upon suppression of AIF1. AIF1 expression is restricted to macrophages, MoDC, and IRF8$^+$ cDC1 but largely absent in IRF4$^+$ cDC2 (12). Suppression of AIF1 in NOD mice resulted in altered frequencies of CD45$^+$CD11b$^+$CD11c$^-$ macrophages and CD45$^+$CD11b$^-$CD11c$^+$ DC compared with control groups (Figure 3A). The total proportion of the CD11b$^+$CD11c$^-$ macrophages was increased from 17.7% in the siScramble control group to 50.5% in the siAIF1 treatment group. There was a markedly lower percentage of CD11b$^-$CD11c$^-$ subsets in the siAIF1-treated group, which is indicative of reduced numbers of infiltrating T cells (Figure 3A). There was a significant reduction in CD11b$^-$CD11c$^+$ DC, with a concomitant increase in the frequency of the CD11b$^+$CD11c$^+$ group, which comprises both macrophages and cDC2 subsets. Collectively, in vivo silencing reduced total levels of AIF1 expression from 24.3% ± 6.1% down to 5.6% ± 2.3% in CD45$^+$ leukocytes within the pancreata of treated NOD mice (Figure 3B).

To further assess alterations of myeloid cells within the pancreata of NOD mice after silencing AIF1, CD45$^+$ cells were sorted for either CD11b$^-$CD11c$^+$F4/80$^-$ DC or CD11b$^+$CD11c$^-$F4/80$^+$ macrophage populations. Cells were then assessed for changes in gene expression by qPCR. In the CD11b$^-$CD11c$^+$F4/80$^-$ DC population, results revealed a significant depression in XCR1, CD103, BATF3, and IRF8, which are each associated with cDC1 phenotypic profiles (Figure 3C). There was a concomitant increase in IRF4 expression. For the sorted CD11b$^+$CD11c$^-$F4/80$^+$ macrophages, transcriptomic profiling also showed
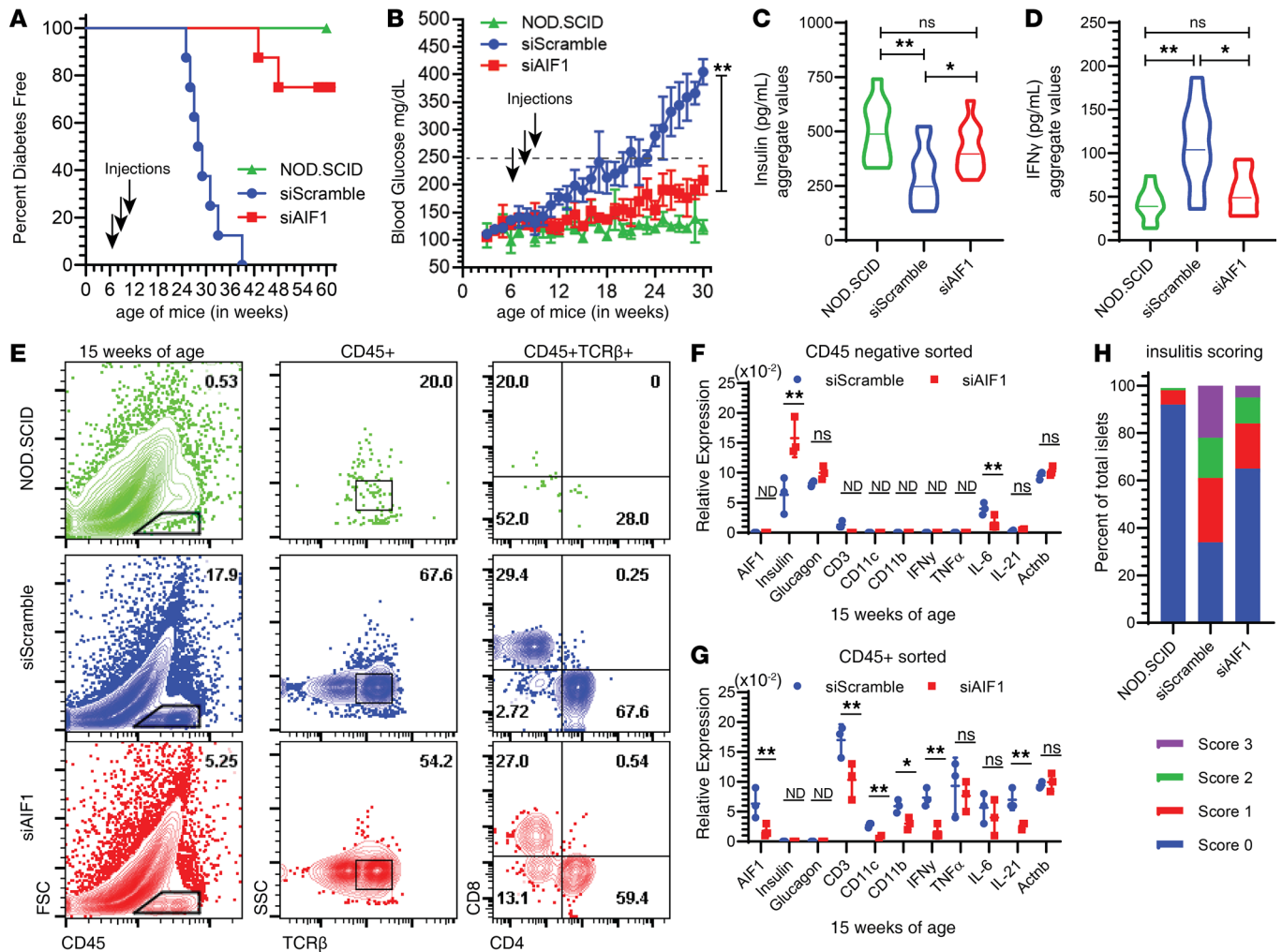
Figure 2. In vivo silencing of AIF1 in NOD mice restrains insulitis. Six-week-old NOD mice were injected i.p. with siRNA targeting AIF1 (siAIF1) (n = 8) (squares) or scrambled control (siScramble) (n = 8) (circles) oligonucleotides weekly for a total of 3 weeks. NOD/SCID mice (triangles) were used as internal controls (n = 8). Treated or control NOD mice were then monitored for (**A**) diabetes onset (presented as percentage free of diabetes) through 60 weeks of age. Arrows denote time points of siRNA i.p. injection. (**B**) Blood glucose levels were monitored weekly through 30 weeks of age. Dashed lane at 250 mg/dL represents the determinant level for diabetes. Arrows denote time points of siRNA i.p. injection. Serum collected biweekly from ages 6 to 30 weeks of NOD/SCID, siScramble, and siAIF1 groups were assessed for (**C**) insulin and IFN-γ (**D**) expression. Data are presented as an aggregate in a violin plot, with the mean represented as a solid line through each plot. Data sets are representative of pooled values with six mice per each cohort. (**E**) At 15 weeks of age (or a total of 9 weeks after initial treatment with siAIF1 or siScramble), mice were sacrificed. Pancreas islets were then isolated before staining for flow cytometric analyses. Dot plots represent FSC vs. CD45, with subsequent plots looking at TCRβ⁺ CD4⁺ vs. CD8⁺ T cell subsets gated from the CD45⁺ leukocyte populations. All gates established using isotype controls. Flow cytometric dot plots data sets are representative of three independent experiments (with 2–3 mice per group). For gene expression analyses, (**F**) CD45ⁿᵉᵍ or (**G**) CD45⁺ subsets from the pancreata of NOD mice were FACS-sorted before performing qPCR analyses. Data are shown as mean ± SEM of three mice per control or treated group and are representative of three independent experiments. (**H**) Insulitis scoring was determined by histological analyses of the pancreas using a graded scale of 0 (no insulitis), 1 (peri-insulitis), 2 (moderate insulitis), or 3 (severe insulitis). Graph shows percentage of each score relative to the total. A total of 40 islets were counted per group. For all graphs, statistical significance was determined by the 2-tailed Student's unpaired t test. *P < 0.05; **P < 0.01. AIF1, allograft inflammatory factor-1; ns, not significant; ND, not determined.

increased levels of IRF4, albeit these were less pronounced (Figure 3D). Further interrogation by gating on the CD45⁺CD11b⁻ population revealed decreased frequency of MHC class II⁺CD11c⁺ subsets; this would largely represent the cDC1 population of DC (Figure 3E). Next, monocyte pools were assessed for infiltration into the islets. By gating on the CD45⁺CD11c⁻CD317⁻ fraction, analyses revealed decreased levels of CD11bʰⁱLy6Cʰⁱ and CD11bʰⁱLy6Cⁱⁿᵗ monocytes in the AIF1-silenced NOD group (Figure 3F). Additionally, there was a moderate increase in the CD11bⁱⁿᵗLy6C⁺ subsets that were F4/80ⁿᵉᵍ. This population has been shown to represent common monocyte progenitors (31). The CD11bʰⁱLy6C⁺ group was positive for F4/80 and represents the mature monocyte pools. Collectively, the percentage of Ly6C⁺ subsets present within the pancreas after in vivo silencing of AIF1 was markedly lower than controls (Figure 3G).
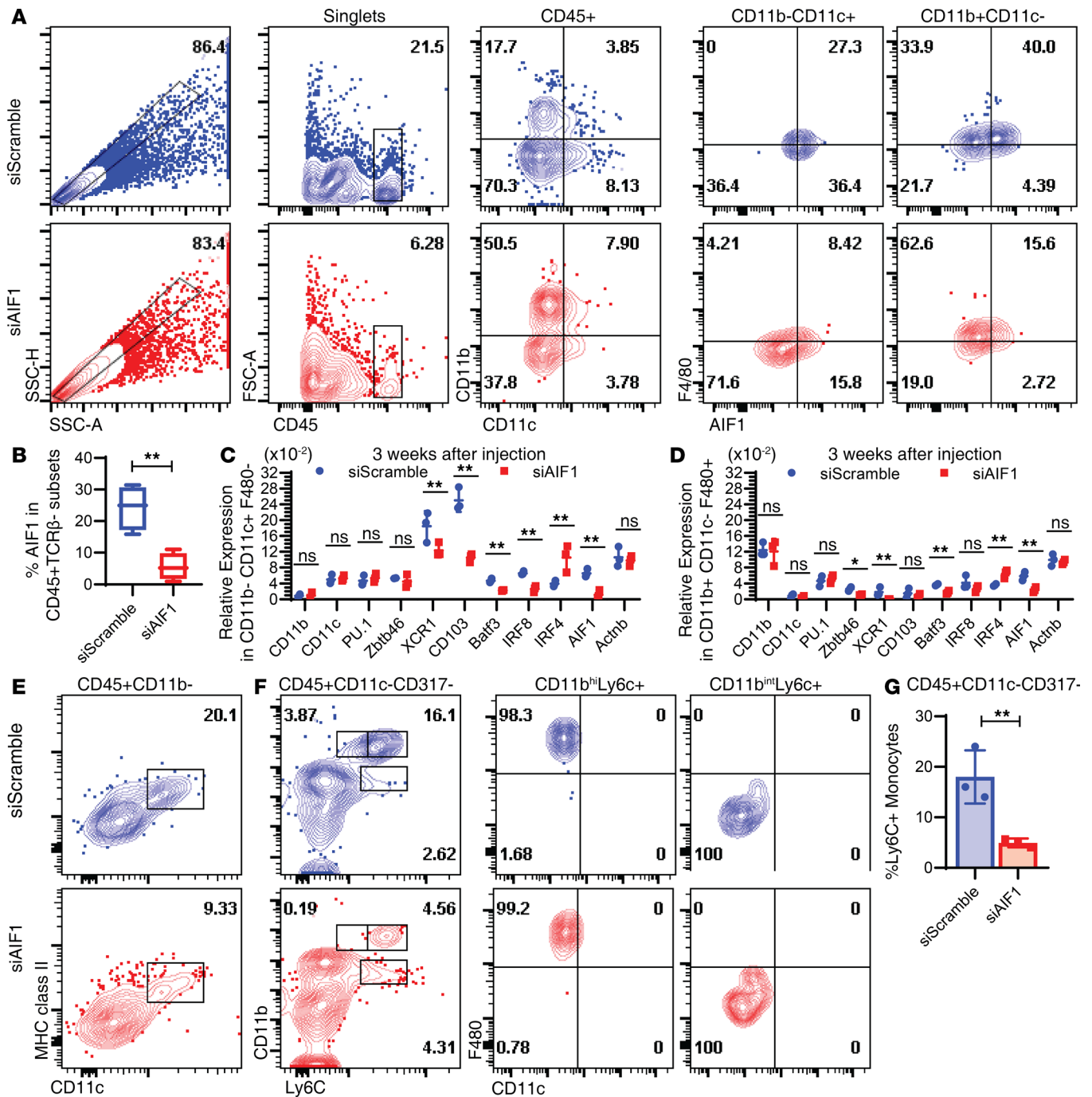
Figure 3. Loss of DC subsets upon in vivo silencing of AIF1 in the pancreas. Six-week-old NOD mice were injected i.p. with siRNA targeting AIF1 (siAIF1) (*n* = 6) or scrambled control (siScramble) (*n* = 5) oligonucleotides weekly for a total of 3 weeks. At the end of the 3 weeks, pancreas was harvested from treated NOD mice and prepared for flow cytometric analyses. (**A**) Cells were stained to assess alterations in the frequency of CD45+CD11b−CD11c+F4/80− DC and CD45+CD11b+CD11c−F4/80+ macrophages upon in vivo silencing of AIF1. SSC-H and SSC-A evaluation was used to identify singlets. Dot plots show CD11b vs. CD11c gating and subgating to assess F4/80 vs. AIF1 expression in gated singlets. (**B**) The average percentage of AIF1 expression was determined in the siScramble vs. siAIF1 among a pool of nine NOD mice from each group across 3 independent experiments. Additionally, expression was assessed in key myeloid-associated genes from pancreatic cells sorted for (**C**) CD45+CD11b−CD11c+F4/80− DC and (**D**) CD45+CD11b+CD11c−F4/80+ macrophages. Data set represents a pool of three siScramble and three siAIF1-treated mice from two independent experiments. Data are presented as mean ± SEM. (**E**) Assessment of MHC class II and CD11c coexpression within pancreas-resident CD45+CD11b− subsets in siScramble vs. siAIF1 cohorts. Data are representative of 4 mice in 2 independent studies. (**F**) Further interrogation of monocyte infiltration through assessment of CD45+CD11c−CD317− fraction showing levels of F4/80 in CD11b^hiLy6c^hi and CD11b^hiLy6c^int monocytes. Figure data sets are representative of two independent experiments. (**G**) Bar graph presenting relative percentage of Ly6C+ monocytes within the CD45+CD11c−CD317− gated subsets in siScramble vs. siAIF1-treated NOD mice. Data are shown as mean ± SEM of 4 groups within 2 independent experiments. Statistical significance was determined by the 2-tailed Student's unpaired *t* test. *P < 0.05; **P < 0.01. AIF1, allograft inflammatory factor-1; ns, not significant.

Reduced infiltration of effector T cells and increased CD25⁺Foxp3⁺ Tregs upon silencing of AIF1. After determining reduced cDC1 and monocyte presence in absence of AIF1, we next assessed alterations in the T cell profile. Mouse pancreata were harvested 3 and 9 weeks after treatment with siAIF1. Results revealed lower levels of CD4⁺TCRβ⁺ T cell infiltration in the islets compared with controls (Figure 4, A and B). There was no marked difference in the CD4⁻TCRβ⁺ subsets 3 weeks after treatment with siAIF1, which chiefly represents the CD8⁺ T cells. However, there was a significant reduction 9 weeks after in vivo AIF1 silencing. This corroborated directly with increased numbers of CD4⁺CD25⁺Foxp3⁺ Treg subsets at both 3 and 9 weeks after treatment with siAIF1. Importantly, there were greater levels of CD4⁺CD25⁺Foxp3⁺ subsets for several weeks after initial treatment with siAIF1 (Figure 4C). Gene expression analyses of pancreas-sorted CD45⁺TCRβ⁺ T cells at 3 weeks after siAIF1 treatment revealed lower levels of the type 1 polarized markers T-bet and IFN-γ, with a concomitant increase in IL-10 and Foxp3 transcript levels in comparison with controls (Figure 4D). There were no significant changes in CD8, Granzyme B, or IL-17A. In evaluating mice 9 weeks after AIF1 silencing, gene expression analyses showed lower levels of IFN-γ and T-bet, with increased levels of Foxp3 in the TCRβ⁺CD45⁺ population (Figure 4E).

Transfer of donor Tregs from in vivo–silenced NOD mice partially rescues recipients from diabetes. Ex vivo–expanded (islet) antigen-specific Tregs adoptively transferred into recipient NOD mice has been shown to serve as effective alleviators of T1D (32–34). Furthermore, silencing AIF1 in DC leads to expansion of antigen-specific Tregs from naive subsets using an ovalbumin transgenic (OT-II) mouse model (13). To evaluate if Tregs from in vivo AIF1-silenced NOD mice were functionally suppressive, CD4⁺CD25⁺CD127⁻ cells were isolated from the pancreata of the siAIF1-treated donor mice and labeled with FarRed labeling dye (Figure 5, A and B). These cells were then adoptively transferred into 6- to 8-week-old recipient NOD mice. For controls, recipient NOD mice received either PBS or ex vivo–expanded polyclonal Tregs derived from the lymph nodes of donor NOD mice. Recipient NOD mice that received the AIF1-silenced pancreatic-resident Tregs, but not the ex vivo polyclonal Treg controls, had lower IFN-γ expression (presented in a condensed aggregate values; Figure 5C), reduced blood glucose levels (Figure 5D), and decreased infiltration of CD45⁺ leukocytes (Figure 5E).

Discussion

This study has established the importance of AIF1 expression within antigen-presenting myeloid cells during insulitis for promotion of T1D. Additionally, our results corroborate those of prior characterization studies, in which higher levels of AIF1 are associated with lower insulin production and increased blood glucose levels in NOD mice (27). Further investigation of the myeloid cell population within the pancreas revealed that AIF1 expression was largely within the CD11c⁺CD11b⁻F4/80⁻MHC class II⁺ DC and CD11b⁺CD11c⁻F4/80⁺ macrophage populations within the pancreas. These findings corroborate the importance of the DC and macrophage subsets during progression of insulitis (2). However, unlike previously published works (27, 35), this study was unable to detect AIF1 expression in blood serum of animals; expression was only detected within myeloid populations.

The principal aim of the previous studies was to evaluate the role of AIF1 in early stages of insulitis. For our study, AIF1⁻/⁻ mice were not crossed on the NOD background as previous work has shown that loss of AIF1 alters hematopoiesis events; blocking AIF1 abrogated generation of cDC and MoDC (12). In turn, this work silenced AIF1 at early stages of autoimmune-driven insulitis. i.p. injection of siRNA using a nonviral liposome-based approach resulted in strong accumulation in myeloid, but not lymphoid, populations within the pancreata of NOD mice (36). A single injection was able to effectively restrain AIF1 expression in CD45⁺ target cells for 7 days. After 9–14 days, there was recovery of endogenous AIF1 expression in myeloid cells within the pancreas compartment. This follows suit with typical observed kinetics of siRNA delivery in nondividing cells (37). Treatment at early time points of 6-week-old early-insulitis prediabetic NOD mice promoted long-term protection by reducing infiltration of effector T cells and increasing the relative number of Tregs in the pancreas. Notably, attempts to silence AIF1 after diabetes onset in NOD mice (i.e., >250 mg/dL; ~>16 weeks of age) did not alleviate the pathology.

Suppressing AIF1 in early stages of insulitis resulted in decreased CD45⁺ leukocytes in the pancreas up to 24 weeks. There was a significant decrease in CD11c⁺ DC numbers and alteration in functional profile of CD4⁺ T helper cells. Three weeks after repetitive weekly in vivo AIF1 silencing in 6-week-old NOD mice resulted in altered frequencies of myeloid and lymphoid cells in the pancreatic islet compartment. Lowered frequencies of CD11c⁺ DC would, in turn, lead to reduced autoantigen presentation
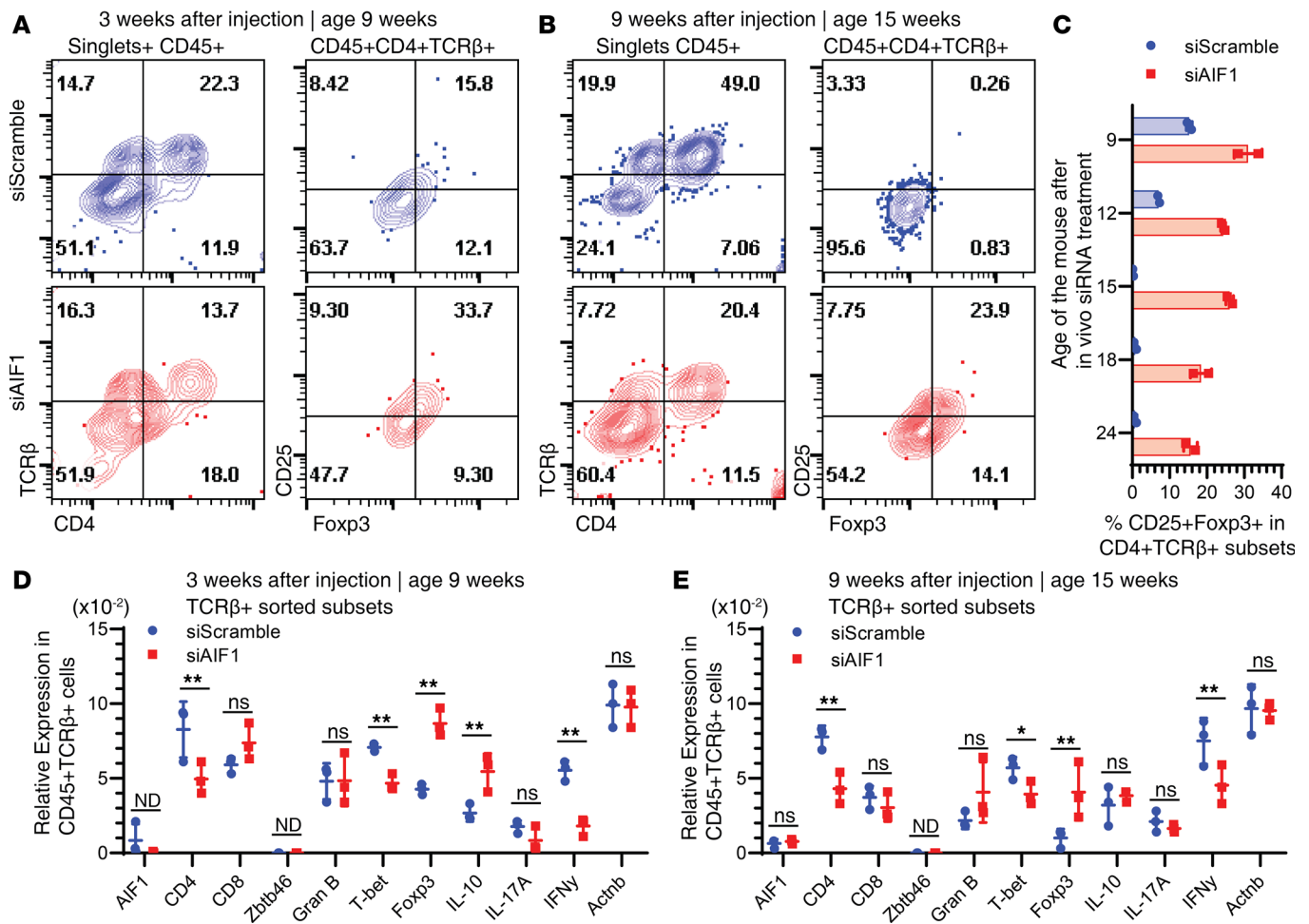
Figure 4. Restrained infiltration of effector T cells and increased expression of CD25+Foxp3+ Tregs upon in vivo silencing of AIF1 in NOD mice. Pancreata from treatment vs. control NOD mice were harvested for 3 or 9 weeks after initial injection of siRNA oligonucleotides targeting AIF1 (siAIF1) (n = 6) or scrambled controls (siScramble) (n = 6). Flow cytometric analysis was performed to assess changes in the CD45+TCRβ+CD4+ T helper population and changes in frequency of CD25+Foxp3+ Tregs (A) 3 weeks or (B) 9 weeks after in vivo AIF1 silencing of NOD mice. Singlets were interrogated by gating SSC-A vs. SSC-H (data not shown). (C) Percentage of CD25+Foxp3+ Tregs was assessed by flow cytometric analyses at 9-, 12-, 15-, 18-, and 24-week-old NOD mice (n = 2 of each time point of each group) after in vivo silencing for AIF1 vs. control oligonucleotides. For gene expression studies, pancreas cells were sorted for CD45+TCRβ+ cells before real-time PCR analyses (D) 3 weeks or (E) 9 weeks after in vivo AIF1 silencing of NOD mice. Statistical significance was determined by the 2-tailed Student's unpaired t test. Data are shown as mean ± SEM of pooled samples of two independent experiments normalized to respective internal loading controls. *$P < 0.05$; **$P < 0.01$. AIF1, allograft inflammatory factor-1; ns, not significant; ND, not determined.

to T cells, thereby restraining infiltration into the islets. Reduced DC infiltration and conversion from monocyte pools would additionally leave macrophages as the dominant myeloid cell within the pancreas, which may explain higher relative frequency of the subsets in AIF1-silenced NOD mice. Furthermore, inhibition of AIF1 expression in the remaining tissue resident macrophages may potentially skew them into an alternative suppressive phenotype, as has been shown in previous reports (16, 38, 39). Finally, given the importance of tissue-infiltrating monocyte-derived macrophages in T1D, silencing of AIF1 could disrupt recruitment and/or monocyte-to-macrophage differentiation (as well as monocyte-to-DC conversion; ref. 12), as observed by the moderate increase in CD11b^{int}Ly6C$^+$F4/80^{neg} cells. Collectively, this would result in impaired antigen presentation capacity and suggest adoption of a tolerogenic state.

Assessment of lymphocytes within the pancreas revealed reduced CD4$^+$ T cell infiltration concomitant with an expanded pool of CD25$^+$Foxp3$^+$ Tregs upon silencing of AIF1. Gene expression analyses also revealed restrained type 1 polarized profiles (i.e., T-bet and IFN-γ) within lymphocytes of AIF1-silenced NOD mice. This may be in part owing to DC transitioning into that of a tolerogenic fate in absence of AIF1 upon autoantigen presentation to cognate T cells (12, 15). The result would be restrained effector functions of T cells and conversion of naive pools into Treg subsets. Suppressive function(s) of the pancreas-resident
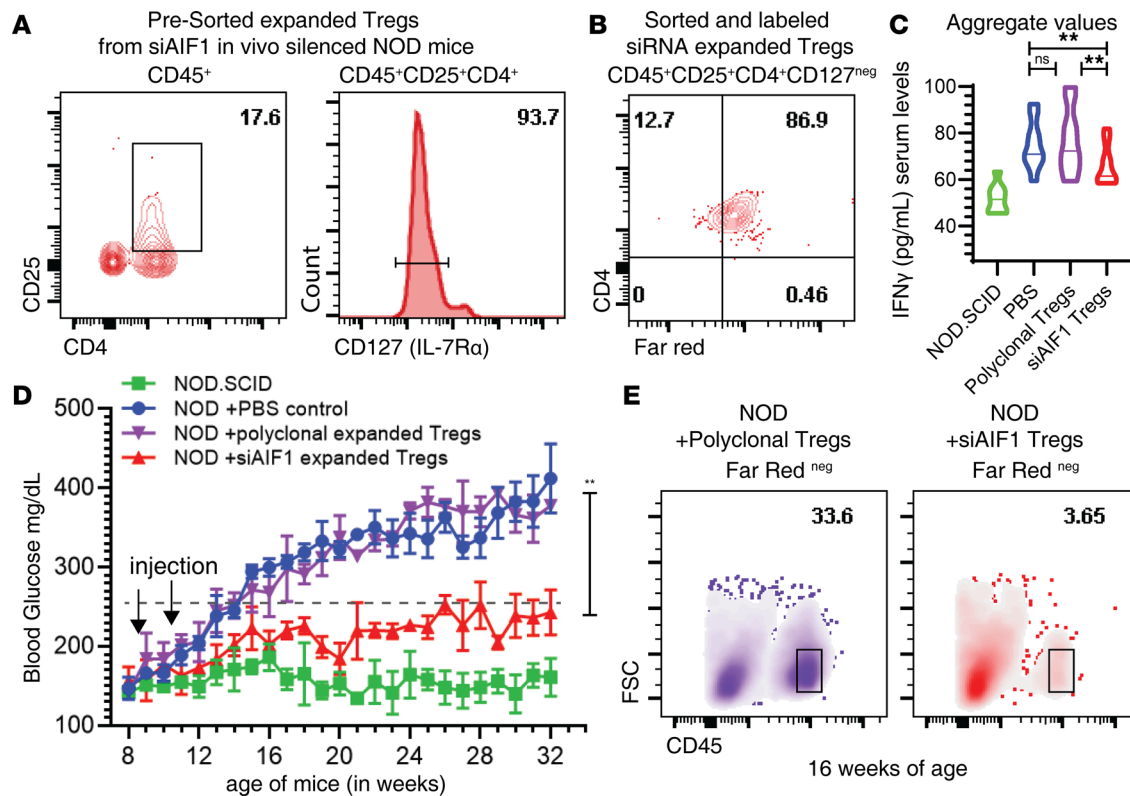
Figure 5. Adoptive transfer of Tregs expanded from AIF1-silenced NOD mice confer protection from insulitis in recipient NOD mice through an antigen specific manner. Six-week-old NOD mice were injected with siRNA targeting AIF1 weekly for 2 weeks to expand pancreas islet-resident TCRβ+CD4+CD25+- Foxp3+. (**A**) To isolate the islet-resident Tregs, CD45+CD4+CD25+CD127- T cells were isolated by flow cytometric sorting and (**B**) labeled with Far Red dye before adoptive transfer. Next, FarRed+ siAIF1-expanded pancreas-resident Tregs (red triangles) or FarRed+ polyclonal Tregs (derived from lymph nodes and subsequently expanded ex vivo using anti-CD3/CD28 +TGF-β for 10 days in culture; purple triangles) were each intravenously injected into recipient NOD mice (*n* = 8) at 8 weeks of age. NOD/SCID (squares) and NOD mice injected with PBS only (circles) served as internal controls. (**C**) IFN-γ and (**D**) glucose levels in the blood were monitored weekly after adoptive transfer of Tregs by ELISA; data for IFN-γ are presented as an aggregate over time period in a violin plot, with the mean represented as solid line through each group. Statistical significance was determined by the 2-tailed Student's unpaired *t* test. *$P < 0.05$; **$P < 0.01$; ns, not significant; ND, not determined. Data are shown as mean ± SEM of three independent experiments. (**E**) Frequency of infiltrating CD45+ leukocytes by flow cytometry was measured in ex vivo–expanded polyclonal Treg vs. in vivo siAIF1-expanded Tregs. FarRed^neg cells were gated out to remove adoptively transferred cells from assessment of the CD45+ leukocyte population within pancreas of recipient NOD mice. AIF1, allograft inflammatory factor-1.

CD25+Foxp3+ T cells expanded by suppressing AIF1 was confirmed upon adoptive transfer of the cells into NOD-recipient mice, which led to restrained autoimmune events. This is important as previous reports established that only islet antigen-specific Foxp3+ Tregs can restrain insulitis (33).

Importantly, Tregs are critical for preventing autoimmune events (40, 41). Patients with T1D have reduced Tregs concomitant with lacking tolerance-regulating DC populations (10). This loss of tolerance drives immune-mediated destruction of the insulin-producing β cells. Several studies have shown that increased presence of islet-specific Foxp3+ Tregs directly suppresses type 1 polarized effector CD4+ T helper cell responses (33, 34). Interestingly, Tonkin et al. reported that autoimmune-induced diabetes can be suppressed by adoptive transfer of expanded polyclonal Tregs (in large enough numbers) owing to the presence of sufficient islet-specific clonal T cells (34). However, in this study, in vivo silencing of AIF1 in NOD mice expanded functionally suppressive islet-autoantigen-specific Tregs within the pancreas. Importantly, transfer of these donor pancreas-resident Tregs to recipient NOD mice prevented onset of T1D. However, expansion of polyclonal Tregs initially isolated from lymph nodes of prediabetic donor NOD mice and transfer into NOD recipients did not limit autoimmune pathology in this study. This result corresponds with other studies that have shown ectopic expression of Foxp3 in polyclonal CD4+ T cells was unable to abrogate T1D (33). Based on the results of this study, it remains plausible to in vitro expand islet-specific Tregs using AIF1-silenced cDC, presenting specific islet antigens during culture for subsequent adoptive transfer into (pre)diabetic recipients as an immunotherapeutic approach.

In conclusion, our study has established that AIF1 expression in antigen-presenting myeloid macrophage and DC subsets is a major contributor to autoimmune-driven insulitis and progression of T1D. Inhibiting AIF1 expression restrains insulitis, alters frequency of antigen-presenting myeloid cells in the pancreatic microenvironment, and expands functionally suppressive Tregs to limit organ-specific pathology. Additionally, our data further support generation of tolerogenic AIF1-deficient DC-based vaccines for expanding autoantigen-specific Tregs or development of small molecule inhibitors targeting the protein as therapeutic tools for restraining insulitis.

Methods

Mice. NOD, NOD.CB17-Prkdcscid/J (NOD/SCID), and C57BL/6 (WT) male and female mice 4–6 weeks of age were used. Mice were purchased from The Jackson Laboratory and housed in pathogen-free facilities. Glucose level monitoring was performed using the Aviva Accu-Check (Roche) glucometer by tail vein prick twice a week to assess diabetes onset and progression. Diabetes incidence was identified as values greater than 250 mg/dL for nonfasted mice after 2 consecutive readings.

In vivo siRNA preparation and injection. In vivo ready (HPLC purified) synthetic was purchased from Life Technologies. Two AIF1 siRNAs (siAIF1) were used: 5′-GGCAAGAGAUCUGCCAUCUUG-3′ and 5′-AGCUGAAGAGAUUAAUUAGAGAGGU-3′. Respective scrambled control siRNA (siScramble); 5′-CCUAUAGAUACCGAGUGGUTT-3′ and 5′-GAATGAAGGGAGTAATCGGTAATAT-3′) served as internal controls. Invivofectamine 3.0 was purchased from Thermo Fisher and used according to the manufacturer's protocol. Stock siAIF1 or siScramble oligonucleotides (at 2.4 mg/mL; 20 nmol) was diluted to 1.2 mg/mL with the complexation buffer (200 μl final) and subsequently combined with Invivofectamine 3.0 reagent (200 μL). The mixed complex was incubated at 50°C for 30 minutes. The siRNA concentration was adjusted to 0.20 mg/mL with PBS. A total of 0.05 mg was injected i.p. into 6-week-old NOD mice. This was equivalent to approximately 2.5 mg/kg weight of the animal. Injections of the siRNA-Invivofectamine mixture into NOD mice were performed 1 week apart. Per each round of experiment, three to four mice per group (i.e., siAIF1 vs. siScramble vs. NOD/SCID) were treated, monitored for diabetes incidence, and had weekly serum collections during the study. This was repeated 3 to 4 times to corroborate and validate reproducibility of findings.

Cryosectioning and fluorescence microscopy. Excised pancreas from treated or control NOD mice were fixed in 3% PFA before transfer into a 50% sucrose solution. Sections were prepared at 10- or 20-μm thickness using an automated cryosectioner (NX70 Cryostat; Thermo Fisher). Preparations were transferred onto poly-L-lysine-coated glass slides. Samples were then permeabilized using 0.3% Triton X-100 solution and blocked with 0.2% BSA in permeabilization buffer. Sections were stained with the following antibodies targeting AIF1 (clone EPR16588) purchased from Abcam and CD11c (clone N418), CD11b (clone M1/70) and CD45 (clone 30-F11) each from BioLegend. Isotype control antibodies were used as internal controls. Last, sections were costained with DAPI (Thermo Fisher) nuclear staining dye before mounting with coverslips. Slides were imaged using a FSX100 fluorescence microscope (Olympus).

Histological examination of insulitis. For quantifying insulitis, the pancreas from control or treated NOD mice were harvested before fixation and cryosectioning. Ten- or twenty-μm-thick sections were prepared before mounting on slides for staining with hematoxylin and eosin (VitroVivo Biotech). The severity of infiltration was assessed by bright-field phase-contrast for at least 40 islets examined per pancreas using the following scoring system: 0, no observable cell infiltration; 1, few infiltrating cells peri-insular (but not infiltrating the islet architecture); 2, moderate infiltration around islet (with less than one-half of islet architecture infiltrated); and 3, large numbers of infiltrating cells (>50% infiltrated leukocytes) within the islet (42).

Isolation of pancreas islets for flow cytometric analyses and sorting. Pancreata from control or treated animals were harvested, islets isolated, and immediately dissociated into single-cell suspension using the GentleMACS Dissociator (Miltenyi) (43). Mouse pancreatic islets were isolated using a standard protocol. Briefly, the pancreas was perfused via the common bile duct to inflation using a 27-g needle with 3 mL collagenase P (MilliporeSigma) in HBSS for 15 minutes of digestion at 37°C before performing Histopaque-1077/1119 (MilliporeSigma) density enrichment gradients, as previously described (44–46). Isolated islets were then dissociated into single-cell suspension in 1 mM EDTA in PBS using the dissociator before straining through a 40-μm cell strainer. Finally, Ammonium-Chloride-Potassium (ACK) lysis buffer was added to remove red blood cells. The approach yielded a viability >90%, as determined by live and/or dead staining.

Flow cytometry and antibodies. Cell surface staining was performed with PBS supplemented with 1 mM EDTA and 2.5% bovine serum (FACS buffer). Islet cells (now in single-cell suspension) were washed with

FACS buffer before extracellular staining with fluorochrome-tagged antibodies. Dilutions were antibody specific, however, roughly 10 μL of a 10 μg/mL working concentration was used per 2×10^5 cells. Respective isotype controls were used in all assays. Cells were then fixed with 3% paraformaldehyde (PFA) in PBS. For intracellular antibody labeling, fixed cells were permeabilized with 0.2% saponin in PBS. Next, primary antibodies or isotype controls were added at approximately 10 μg/mL concentrations followed by washing and subsequent staining with secondary fluorochrome-labeled antibodies. Antibodies used in the experiments included: CD45 (clone 30-F11), CD11c (clone N418), CD11b (clone M1/70), F4/80 (clone BM8), TCR- β chain (clone H57-597), CD8 (clone 53-6.7), CD4 (clone RM4-5), CD25 (clone PC61), Foxp3 (clone MF14), CD127 (clone A7R34), MHC class II (I-A^{g7}; clone 10-3-.6), PDCA-1/CD317 (clone SA376A4), and Ly6C (clone HK1.4). All antibodies were purchased from BioLegend. Cells were acquired on a BD FACSVerse flow cytometric analyzer (BD Biosciences). Characterization approaches to islet leukocyte populations were in part followed by prior published methodologies (47–49). Data sets were analyzed using Flow Jo v10 (Flow Jo LLC). All quadrilateral polygons in respective dot plots identifying the subpopulation of cells were further interrogated. Text labeling above the flow cytometry dot plots represent the analyzed population (i.e., pregated populations). Doublets were excluded from analyses using both SSC-A versus SSC-H and FSC-A versus FSC-H gating approaches.

FACS and qPCR. Pancreas was harvested from treated or control NOD mice groups. Single-cell suspension was then prepared using the GentleMACS Dissociator. Cells were treated with ACK lysis buffer before resuspension in PBS buffer with 1 mM EDTA. Cells were then stained with CD45, TCRβ, CD4, CD25, CD11c, MHC class II (I-A^{g7}), CD103, CD11b, and/or F480 for flow cytometric sorting of T cells, DC or macrophages. Sorted subsets were then immediately transferred to TRIzol reagent for RNA isolation before reverse transcription. Prepared cDNA was then amplified and measured using the Thermo Fisher QuantStudio 5. The following TaqMan probes were used: AIF1 (Mm00479862_g1), BATF3 (Mm00479410_m1), ACTB (Mm02619580_g1), ITGAE (CD103; Mm00434443_m1), CD11b (ITGAM; Mm00434455_m1), CD11c (ITGAX; Mm00498701_m1), CD4 (Mm00442754_m1), CD8α (Mm01182108_m1), Foxp3 (Mm00475162_m1), GZMB (Mm00442837_m1), IL-10 (Mm01288386_m1), insulin (Mm00731595_gH), IFN-γ (Mm01168134_m1), IL-17A (Mm00439618_m1), TBX21 (T-bet; Mm00450960_m1); TNF-α (Mm00443258_m1), Glucagon (GCG; Mm00801714_m1), IL-6 (Mm00446190_m1), PU.1 (Mm00488140_m1), Zbtb46 (Mm00511327_m1), IRF4 (Mm00516431_m1), and IRF8 (Mm00516431_m1). β-Actin (Mm02619580_g1) or GAPDH (Mm99999915_g1) was used to normalize candidate gene expression and measure fold changes among groups.

Glucose monitoring and serum collection. Mice tails were pricked to collect 2 μL of blood for immediate reading on glucometer test strips and 10 μL for sera collection weekly. Samples were diluted in PBS when glucose levels exceeded detection threshold by an Aviva Accu-Chek glucometer.

Luminex multiplex analyses. Serum samples were added to a mixture of beads precoated with analyte-specific capture antibody. Biotinylated detection antibody specific to the analyte was added to form the antibody-antigen sandwich before reading on the Luminex MAGPIX Analyzer (Luminex). Luminex Th1/Th2/Th9/Th17/Th22/Treg Cytokine 17-Plex Mouse ProcartaPlex Panel was used (Thermo Fisher).

Adoptive transfer of Tregs. NOD mice in vivo–silenced with AIF1 at 6, 7, and 8 weeks of age were sacrificed 8–9 weeks after initial treatment (14–15 weeks of age). These mice served as donors. Pancreas was isolated into single-cell suspension using the GentleMACS Dissociator before staining with antibodies to CD45, CD25, CD4, and CD127. To acquire enough numbers, 2–3 pancreata from donor AIF1-silenced NOD mice were pooled together. CD45$^+$CD4$^+$CD25$^+$CD127^{neg} subsets were then sorted by FACS and labeled with Far Red labeling dye (Thermo Fisher). This group represents isolated pancreas-resident Tregs from NOD mice silenced for AIF1. For generation of polyclonal expanded Tregs that are not antigen-specific, lymph nodes of 6-week-old NOD mice were harvested before purification of CD4$^+$ T cells using negative depletion of CD8$^+$ and MHC class II$^+$ cells. This resulted in a 96.3% ± 1.4% purity of CD4$^+$CD69$^-$CD62L$^+$ naive T cells as assessed by flow cytometric analyses. These naive CD4$^+$ T cells were then cultured with αCD3/CD28 coated beads (Dynabeads; Thermo Fisher Scientific) and TGF-β cytokine in the presence of neutralizing antibodies to IFN-γ, IL-12, and IL-4 for 10 days, with IL-2 added to the culture beginning on day 3. A fraction of the polyclonal expanded cells was isolated and confirmed for >95% of cells being CD4$^+$Foxp3$^+$CD25$^+$T-bet$^-$. At the end of the culture, these expanded polyclonal Tregs were labeled with Far Red dye. For adoptive transfer into recipient NOD mice, Far Red-labeled siAIF1 in vivo-derived or ex vivo polyclonal-expanded Tregs from NOD donors were then resuspended in PBS at 10^6 cells/100 μL. Intravenous injection of 250 μL of Tregs into recipient NOD

mice was at indicated time points. Mice were then monitored for glucose weekly and serum collected for metabolic indices measured by Luminex and ELISA.

Statistics. GraphPad Prism v8.0 (GraphPad Software) was used to determine statistical significance and generate graphs. The 2-tailed Student's unpaired *t* test was used to evaluate the significance of 2 groups. A 1-way or 2-way ANOVA was used to evaluate the significance between the means of 3 or more independent groups. Significance of differences between groups was tested by comparing group means and medians (mean survival time) by either the 2-tailed Student's *t* test or Wilcoxon's signed-rank test, as appropriate. A *P* value of less than 0.05 was considered statistically significant. The data represent the mean ± SEM of 3 independent experiments.

Study approval. All animal studies were approved by the Institutional Animal Care and Use Committee (IACUC) through the Office of Regulatory Research and Compliance at Howard University, Washington, DC, USA.

Author contributions

DE and ML designed the overall research. DE, NB, RS, and ML conducted experiments, acquired data, and analyzed the results. DE, TM, and ML wrote the manuscript. ML supervised the project.

Acknowledgments

Address correspondence to: Michael Lipscomb, 415 College Street NW, Washington, DC 20059, USA. Phone: 202.806.7939; Email: michael.lipscomb@howard.edu.

1. Anderson MS, Bluestone JA. The NOD mouse: a model of immune dysregulation. *Annu Rev Immunol*. 2005;23:447–485.
2. Ferris ST, Carrero JA, Mohan JF, Calderon B, Murphy KM, Unanue ER. A minor subset of Batf3-dependent antigen-presenting cells in islets of Langerhans is essential for the development of autoimmune diabetes. *Immunity*. 2014;41(4):657–669.
3. Arnush M, Scarim AL, Heitmeier MR, Kelly CB, Corbett JA. Potential role of resident islet macrophage activation in the initiation of autoimmune diabetes. *J Immunol*. 1998;160(6):2684–2691.
4. Klementowicz JE, et al. Cutting Edge: origins, recruitment, and regulation of CD11c^{+} cells in inflamed islets of autoimmune diabetes mice. *J Immunol*. 2017;199(1):27–32.
5. Carrero JA, et al. Resident macrophages of pancreatic islets have a seminal role in the initiation of autoimmune diabetes of NOD mice. *Proc Natl Acad Sci U S A*. 2017;114(48):E10418–E10427.
6. Turley S, Poirot L, Hattori M, Benoist C, Mathis D. Physiological beta cell death triggers priming of self-reactive T cells by dendritic cells in a type-1 diabetes model. *J Exp Med*. 2003;198(10):1527–1537.
7. Hugues S, et al. Tolerance to islet antigens and prevention from diabetes induced by limited apoptosis of pancreatic β cells. *Immunity*. 2002;16(2):169–181.
8. Satpathy AT, et al. Zbtb46 expression distinguishes classical dendritic cells and their committed progenitors from other immune lineages. *J Exp Med*. 2012;209(6):1135–1152.
9. Pop SM, Wong CP, Culton DA, Clarke SH, Tisch R. Single cell analysis shows decreasing FoxP3 and TGFβ1 coexpressing CD4^{+}CD25^{+} regulatory T cells during autoimmune diabetes. *J Exp Med*. 2005;201(8):1333–1346.
10. Badami E, et al. Defective differentiation of regulatory FoxP3^{+} T cells by small-intestinal dendritic cells in patients with type 1 diabetes. *Diabetes*. 2011;60(8):2120–2124.
11. Liu G, Ma H, Jiang L, Zhao Y. Allograft inflammatory factor-1 and its immune regulation. *Autoimmunity*. 2007;40(2):95–102.
12. Elizondo DM, et al. Allograft inflammatory factor-1 governs hematopoietic stem cell differentiation into cDC1 and monocyte-derived dendritic cells through IRF8 and RelB in vitro. *Front Immunol*. 2019;10:173.
13. Elizondo DM, Andargie TE, Yang D, Kacsinta AD, Lipscomb MW. Inhibition of allograft inflammatory factor-1 in dendritic cells restrains CD4^{+} T cell effector responses and induces CD25^{+}Foxp3^{+} T regulatory subsets. *Front Immunol*. 2017;8:1502.
14. Utans U, Arceci RJ, Yamashita Y, Russell ME. Cloning and characterization of allograft inflammatory factor-1: a novel macrophage factor identified in rat cardiac allografts with chronic rejection. *J Clin Invest*. 1995;95(6):2954–2962.
15. Elizondo DM, Andargie TE, Haddock NL, da Silva RLL, de Moura TR, Lipscomb MW. IL-10 producing CD8^{+} CD122^{+} PD-1^{+} regulatory T cells are expanded by dendritic cells silenced for Allograft Inflammatory Factor-1. *J Leukoc Biol*. 2019;105(1):123–130.
16. Yang ZF, et al. Allograft inflammatory factor-1 (AIF-1) is crucial for the survival and pro-inflammatory activity of macrophages. *Int Immunol*. 2005;17(11):1391–1397.
17. Watano K, et al. Allograft inflammatory factor-1 augments production of interleukin-6, -10 and -12 by a mouse macrophage line. *Immunology*. 2001;104(3):307–316.
18. Ito D, Imai Y, Ohsawa K, Nakajima K, Fukuuchi Y, Kohsaka S. Microglia-specific localisation of a novel calcium binding protein, Iba1. *Brain Res Mol Brain Res*. 1998;57(1):1–9.
19. Schluesener HJ, Seid K, Kretzschmar J, Meyermann R. Allograft-inflammatory factor-1 in rat experimental autoimmune encephalomyelitis, neuritis, and uveitis: expression by activated macrophages and microglial cells. *Glia*. 1998;24(2):244–251.

20. Otieno FG, Lopez AM, Jimenez SA, Gentiletti J, Artlett CM. Allograft inflammatory factor-1 and tumor necrosis factor single nucleotide polymorphisms in systemic sclerosis. *Tissue Antigens*. 2007;69(6):583–591.

21. Alkassab F, et al. An allograft inflammatory factor 1 (AIF1) single nucleotide polymorphism (SNP) is associated with anti-centromere antibody positive systemic sclerosis. *Rheumatology (Oxford)*. 2007;46(8):1248–1251.

22. Pawlik A, et al. Effect of allograft inflammatory factor-1 gene polymorphisms on rheumatoid arthritis treatment with methotrexate. *Postepy Hig Med Dosw (Online)*. 2013;67:637–642.

23. Pawlik A, et al. Allograft inflammatory factor-1 gene polymorphisms in patients with rheumatoid arthritis. *Genet Test Mol Biomarkers*. 2012;16(5):341–345.

24. Chinnasamy P, et al. Loss of allograft inflammatory factor-1 ameliorates experimental autoimmune encephalomyelitis by limiting encephalitogenic CD4 T-cell expansion. *Mol Med*. 2015;21:233–241.

25. Eike MC, et al. Genetic variants of the HLA-A, HLA-B and AIF1 loci show independent associations with type 1 diabetes in Norwegian families. *Genes Immun*. 2009;10(2):141–150.

26. Nishimura M, et al. TNF, TNF receptor type 1, and allograft inflammatory factor-1 gene polymorphisms in Japanese patients with type 1 diabetes. *Hum Immunol*. 2003;64(2):302–309.

27. Zhao YY, Huang XY, Chen ZW. Daintain/AIF-1 (Allograft Inflammatory Factor-1) accelerates type 1 diabetes in NOD mice. *Biochem Biophys Res Commun*. 2012;427(3):513–517.

28. Chen ZW, et al. Identification, isolation, and characterization of daintain (allograft inflammatory factor 1), a macrophage polypeptide with effects on insulin secretion and abundantly present in the pancreas of prediabetic BB rats. *Proc Natl Acad Sci U S A*. 1997;94(25):13879–13884.

29. Donovan KM, et al. Allograft inflammatory factor 1 as an immunohistochemical marker for macrophages in multiple tissues and laboratory animal species. *Comp Med*. 2018;68(5):341–348.

30. Orsmark C, Skoog T, Jeskanen L, Kere J, Saarialho-Kere U. Expression of allograft inflammatory factor-1 in inflammatory skin disorders. *Acta Derm Venereol*. 2007;87(3):223–227.

31. Hettinger J, et al. Origin of monocytes and macrophages in a committed progenitor. *Nat Immunol*. 2013;14(8):821–830.

32. Tenspolde M, et al. Regulatory T cells engineered with a novel insulin-specific chimeric antigen receptor as a candidate immunotherapy for type 1 diabetes. *J Autoimmun*. 2019;103:102289.

33. Jaeckel E, von Boehmer H, Manns MP. Antigen-specific FoxP3-transduced T-cells can control established type 1 diabetes. *Diabetes*. 2005;54(2):306–310.

34. Tonkin DR, He J, Barbour G, Haskins K. Regulatory T cells prevent transfer of type 1 diabetes in NOD mice only when their antigen is present in vivo. *J Immunol*. 2008;181(7):4516–4522.

35. Fukui M, et al. Serum allograft inflammatory factor-1 is a novel marker for diabetic nephropathy. *Diabetes Res Clin Pract*. 2012;97(1):146–150.

36. Leconet W, Petit P, Peraldi-Roux S, Bresson D. Nonviral delivery of small interfering RNA into pancreas-associated immune cells prevents autoimmune diabetes. *Mol Ther*. 2012;20(12):2315–2325.

37. Bartlett DW, Davis ME. Insights into the kinetics of siRNA-mediated gene silencing from live-cell and live-animal bioluminescent imaging. *Nucleic Acids Res*. 2006;34(1):322–333.

38. Yang ZF, et al. Antiinflammatory properties of IL-10 rescue small-for-size liver grafts. *Liver Transpl*. 2007;13(4):558–565.

39. Sommerville LJ, Xing C, Kelemen SE, Eguchi S, Autieri MV. Inhibition of allograft inflammatory factor-1 expression reduces development of neointimal hyperplasia and p38 kinase activity. *Cardiovasc Res*. 2009;81(1):206–215.

40. Schubert LA, Jeffery E, Zhang Y, Ramsdell F, Ziegler SF. Scurfin (FOXP3) acts as a repressor of transcription and regulates T cell activation. *J Biol Chem*. 2001;276(40):37672–37679.

41. Hori S, Nomura T, Sakaguchi S. Control of regulatory T cell development by the transcription factor Foxp3. *Science*. 2003;299(5609):1057–1061.

42. Bour-Jordan H, Salomon BL, Thompson HL, Santos R, Abbas AK, Bluestone JA. Constitutive expression of B7-1 on B cells uncovers autoimmunity toward the B cell compartment in the nonobese diabetic mouse. *J Immunol*. 2007;179(2):1004–1012.

43. Epshtein A, Sakhneny L, Landsman L. Isolating and analyzing cells of the pancreas mesenchyme by flow cytometry. *J Vis Exp*. 2017;(119).

44. Pechhold K, et al. Dynamic changes in pancreatic endocrine cell abundance, distribution, and function in antigen-induced and spontaneous autoimmune diabetes. *Diabetes*. 2009;58(5):1175–1184.

45. Clardy SM, et al. Rapid, high efficiency isolation of pancreatic ß-cells. *Sci Rep*. 2015;5:13681.

46. Gotoh M, Maki T, Kiyoizumi T, Satomi S, Monaco AP. An improved method for isolation of mouse pancreatic islets. *Transplantation*. 1985;40(4):437–438.

47. Butcher MJ, Trevino MB, Imai Y, Galkina EV. Characterization of islet leukocyte populations in human and murine islets by flow cytometry. *Methods Mol Biol*. 2020;2076:185–197.

48. Faveeuw C, Gagnerault MC, Lepault F. Isolation of leukocytes infiltrating the islets of Langerhans of diabetes-prone mice for flow cytometric analysis. *J Immunol Methods*. 1995;187(1):163–169.

49. Zinselmeyer BH, Vomund AN, Saunders BT, Johnson MW, Carrero JA, Unanue ER. The resident macrophages in murine pancreatic islets are constantly probing their local environment, capturing β cell granules and blood particles. *Diabetologia*. 2018;61(6):1374–1383.